Journal of Metals, Materials and Minerals, 37(1), e2790, 2027

Effect of quenching atmosphere on surface morphology, hardness, and adhesion of diamond-like carbon (DLC) coatings on SUJ2 steel

Manusavee TAKSADEJ[1,2], Patama VISUTTIPITUKUL[1], Prasonk SRICHAROENCHAI[1], Jatupon OPAPAIBOON[1], Nipon TAWEEJUN[2] and Nithi SAENARJHAN[1,*]

[1] *Department of Metallurgical Engineering, Faculty of Engineering Chulalongkorn University, Bangkok, 10330, Thailand*
[2] *Thai Tohken Thermo Co., Ltd, Chonburi, 20000, Thailand*

***Corresponding author e-mail**: Nithi.S@chula.ac.th

Received date:
23 June 2026
Revised date:
22 July 2026
Accepted date:
29 September 2026

Keywords:
SUJ2 steel;
Quenching;
Tempering;
Microcracks;
DLC coating

Abstract

Diamond-like carbon (DLC) coatings were deposited on hardened SUJ2 steel subjected to two different quenching process atmospheres: gas-controlled and low-pressure conditions. In this study, a hybrid PVD/PE-CVD technique was employed to fabricate the DLC coating films, aiming to enhance surface hardness and improve tribological performance. The effects of quenching atmosphere on surface integrity and coating performance were evaluated using SEM, Raman spectroscopy, surface profilometry, Vickers hardness and dynamic ultra-micro hardness tests, coating thickness measurement, and scratch testing. SEM observation revealed microcracks on gas-quenched surfaces, while low-pressure quenched specimens werecrack-free. Raman spectra confirmed successful DLC deposition on all samples through the presence of characteristic D and G bands. Although substrate hardness was similar, the presence of microcracks led to non-uniform coatings, reduced hardness by approximately 400 Hv, increased thickness, and affected adhesion behaviour (higher Lc1 but lower Lc2). In contrast, low-pressure quenching resulted in uniform coatings with higher Lc2 values, indicating improved adhesion. These findings indicate that low-pressure quenching enhances surface integrity and optimizes DLC coating performance. Additionally, it offers industrial advantages, including reduced polishing requirements, shorter processing time, and lower production costs.

1. Introduction

Owing to its excellent hardness and wear resistance SUJ2 bearing steel (JIS G4805) is widely used in the production of automotive components [1], particularly in applications such as bearings, high-pressure fuel injector parts, and other pressure-generating elements. To meet specific mechanical property requirements, these components undergo various heat treatment processes depending on the initial steel grade. In addition, surface coating techniques such as Physical Vapor Deposition (PVD) and Plasma-Enhanced Chemical Vapor Deposition (PE-CVD) are commonly applied to further enhance performance and extend service life [2–5].

The manufacturing supply chain for automotive components typically includes material selection, cutting and forming, heat treatment, surface finishing, coating, and final assembly. Among these processes, heat treatment plays a critical role in determining the final properties of SUJ2 steel. A commonly employed method involves austenitization under a controlled gas atmosphere followed by oil quenching [6]. In this process, the material is heated to approximately 810°C to 850°C to form austenite and is subsequently quenched in oil at 60°C to 120°C to produce a martensitic structure. This is followed by tempering at approximately 150°C to 200°C to obtain tempered martensite, thereby improving toughness while maintaining high hardness.

To further improve surface hardness and reduce friction, Diamond-Like Carbon (DLC) coatings are widely applied. A hybrid coating technique is commonly used, in which an interlayer is first deposited by PVD, followed by DLC deposition using PE-CVD [1]. Prior to coating, the substrate surface is cleaned using ultrasonic cleaning with solvent-based solutions. During the coating process, the components are placed in a vacuum chamber and heated to approximately 200°C to remove residual moisture and contaminants. Argon ion sputtering is then performed to eliminate native oxide layers, after which the interlayer and DLC coating are sequentially deposited [2,3,7,8].

Although the hardening process under a gas-controlled atmosphere is widely adopted due to its cost-effectiveness and ease of process control, it still presents certain limitations. In particular, it can lead to internal oxidation on the material surface [9–11]. This phenomenon may result in the formation of surface microcracks during hardening, which adversely affect subsequent processing steps. These microcracks necessitate additional surface preparation, such as polishing, prior to coating or application, as they can significantly reduce coating quality, uniformity, and adhesion.

Therefore, this study focuses on investigating methods to eliminate surface microcracks formed after hardening under both gas-controlled and low-pressure atmosphere conditions. The specimens are then subjected to different surface preparation conditions: no polishing,

conventional mechanical polishing, and polishing aimed at microcracks removal. All specimens are subsequently coated with DLC to evaluate various properties, including microcrack formation, Raman characteristics, surface roughness, substrate hardness, coating hardness, coating thickness, and coating adhesion. The ultimate objective is to minimize or eliminate the need for surface polishing prior to coating, thereby reducing manufacturing steps, processing time, and overall production costs.

2. Materials and experimental procedure

JIS SUJ2 bearing steel [12] was subjected to a spheroidizing anneal and subsequently used as the base material. The resulting microstructure, consisting of a ferritic matrix with spheroidal carbides, was confirmed by SEM analysis (JEOL, JXA-ISP100), as shown in Figure 1. The material was then machined into cylindrical specimens with dimensions of Ø20 mm × 7 mm. The chemical composition, in accordance with the JIS standard, is presented in Table 1. Prior to hardening, surface preparation, and DLC coating, the specimen surfaces were finished to an average surface roughness of approximately Ra ≈ 0.20 μm.

The specimens were austenitized at 830°C for 120 min, followed by oil quenching at 100°C and tempering at 180°C for 120 min [6]. Two quenching atmospheres were employed: a gas-controlled atmosphere (GQT) and a low-pressure vacuum condition (VQT), as illustrated in Figure 2, respectively. Following heat treatment, the specimens were subjected to three distinct surface preparation conditions to assess the influence of surface state on coating behaviour: (i) no polishing (N), (ii) conventional mechanical polishing (P), and (iii) polishing aimed at microcracks removal (PM). Prior to coating deposition, all specimens were ultrasonically cleaned in a solvent-based oil to eliminate residual contaminants and ensure surface cleanliness. Diamond-like carbon (DLC) coatings were subsequently deposited using a hybrid physical vapor deposition (PVD) and plasma-enhanced chemical vapor deposition (PE-CVD) process at approximately 200°C, employing acetylene (C_2H_2) and argon (Ar) as precursor gases. For systematic identification, the specimens were designated according to their heat treatment and surface preparation conditions as follows: (i) RM for raw material, (ii) GQT-N for gas-controlled atmosphere quenching and tempering without polishing, (iii) GQT-P for gas-controlled atmosphere quenching and tempering with conventional mechanical polishing, (ix) GQT-PM for gas-controlled atmosphere quenching and tempering with polishing aimed at microcracks removal, (x) VQT-N for vacuum quenching and tempering without polishing, (xi) VQT-P for vacuum quenching and tempering with conventional mechanical polishing, and (xii) VQT-PM for vacuum quenching and tempering with polishing aimed at microcracks removal.

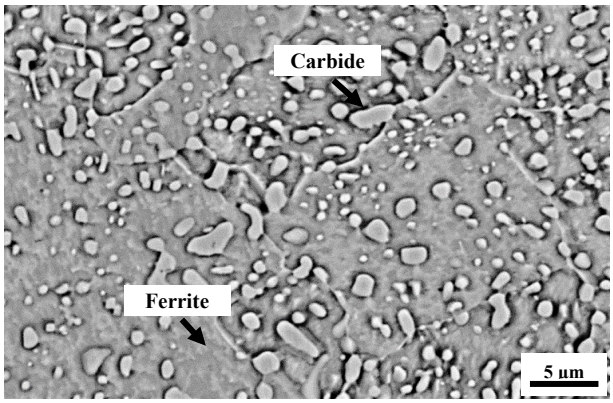


Figure 1. Microstructure of the as-received base material by Nital5% (annealed SUJ2 steel).

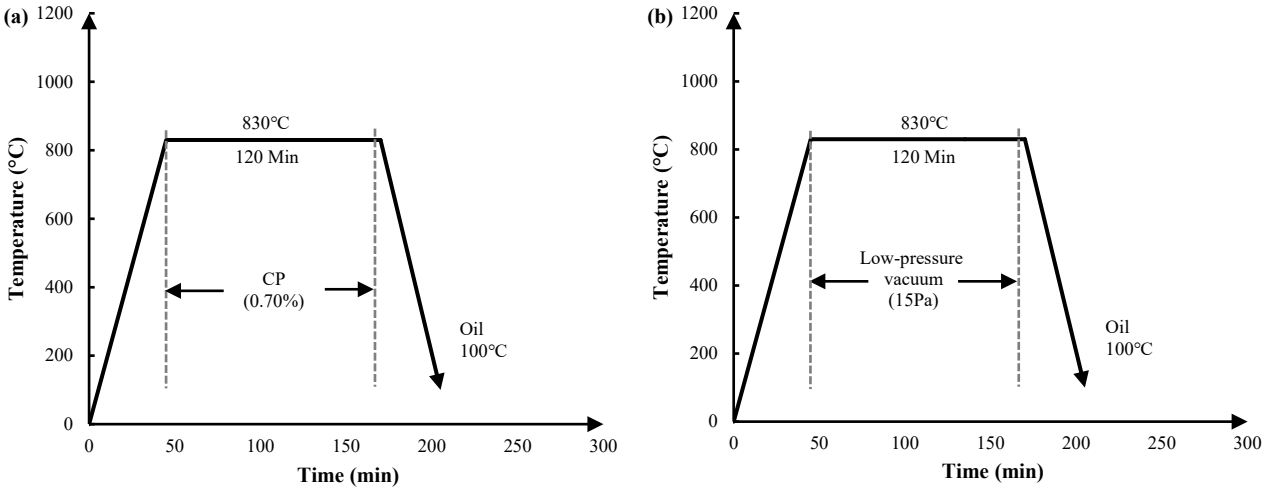


Figure 2. Schematic of quenching parameters: (a) gas-controlled atmosphere (GQT), and (b) low-pressure vacuum atmosphere (VQT).

Table 1. Chemical composition of base material (SUJ2 steel).

Material	Chemical composition [wt%]								
	C	Si	Mn	P	S	Cu	Ni	Cr	Mo
JIS standard	0.95 to 1.10	0.15 to 0.35	< 0.50	< 0.025	< 0.025	< 0.25	< 0.25	1.30 to 1.60	< 0.08
Test Specimen	0.99	0.30	0.31	0.011	0.001	0.10	0.06	1.38	0.03

For microstructural observation and scanning electron microscopy (SEM) analysis, the specimens were sectioned using a fiber cutting wheel under water cooling to minimize heat generation and prevent microstructural alteration. The cut samples were subsequently ground using a series of abrasive papers with progressively finer grits, followed by polishing with an alumina suspension on a felt cloth until a smooth, scratch-free surface was obtained. The polished specimens were then etched with 5% Nital solution to reveal the microstructure. Microstructural characterization was performed using an optical microscope (OM; Nikon corporation, MM-400U) and a scanning electron microscope (SEM; JEOL, JXA-ISP100). The structural characteristics of the DLC coatings were analyzed by Raman spectroscopy (Horiba, XploRA™ PLUS) to identify the D and G bands. Surface roughness (Ra) was measured using a surface roughness tester (Accretech Surfcom, TOUCH 50). The hardness of the substrate was evaluated using a micro-vickers hardness tester (Future tech, FM-800) under a load of 2.94 N (0.3 kgf), while the hardness of the DLC coatings was determined using a dynamic ultra-microhardness tester (Shimadzu, DUH-211S) equipped with a Berkovich indenter. To evaluate the mechanical response of the coating-substrate system, measurements were conducted in a depth-controlled mode set at a penetration depth (h) of 0.300 μm. This condition was selected to determine the apparent composite hardness of the DLC/substrate system and to assess the influence of underlying substrate defects, such as microcracks in the GQT-N condition. The thickness of the DLC coatings was measured by the Calotest method (CSM Instruments, CALOTEST®). Adhesion properties of the coatings were evaluated using a scratch tester (Bruker, UMT TriboLab) under a progressively increasing load from 0 to 100 N over a scratch length of 5 mm. All measurements, including hardness, coating thickness, surface roughness, and scratch testing, were performed five times for each specimen to ensure reproducibility.

3. Results and discussion

3.1 Microstructure

The optical micrographs (OM) of the specimens after gas-quenched treating (GQT) and vacuum-quenched treating (VQT) are shown in Figure 3. The results indicate that the dominant microstructure consists of tempered martensite and spheroidized carbides, with no significant differences observed between the two processes. However, OM observation with limited magnification were not sufficient to clearly detect microcracks in the specimen surfaces. Therefore, further examination was conducted using a scanning electron microscopy (SEM), as shown in Figure 4. The SEM results reveal that specimens treated by GQT exhibit evident surface microcracks, whereas no such microcracks are observed in specimens treated by VQT. This behavior can be explained by the formation of an internal oxidation layer depth near the surface during the GQT process directly interpreted through the metallurgical mechanisms elucidated by previous investigators [9–11], which induces residual stress and leads to the formation of microcracks. In contrast, the VQT process can reduce or prevent the formation of such oxidation layers, thereby avoiding microcrack formation on the surface.

Conversely, as demonstrated by the crack-free morphology of the VQT specimens, the low-pressure vacuum environment successfully suppresses or entirely mitigates the formation of such detrimental oxidation layers, thereby preventing stress-induced surface cracking. It is worth noting that despite these surface-level microstructural variations, both quenching techniques yield equivalent bulk microstructural properties. Therefore, both substrates remain metallurgically viable for subsequent DLC coating deposition, irrespective of the initial surface cracking state or the variation in post-quenching surface preparation conditions.

As presented in the cross-sectional EPMA quantitative elemental maps of Figure 5 and Figure 6, severe enrichment of oxygen (O), chromium (Cr), and silicon (Si) is clearly detected along the microcracks located beneath the outermost coating layer in the GQT-N specimen. This elemental accumulation corresponds to the precipitation of chromium and silicon oxides along the prior austenite grain boundaries, which induces localized volumetric expansion and severe grain boundary embrittlement. Consequently, these preferential intergranular oxidation sites act as primary failure initiation zones during the gas quenching process, leading to microcrack formation. In contrast, beneath the outermost coating layer the VQT-N specimen exhibits a crack-free surface morphology accompanied by a uniformly distributed, profile of O, Cr, and Si across the surface-adjacent layer. This contrast confirms that low-pressure vacuum quenching effectively suppresses internal oxidation, thereby eliminating grain boundary degradation and preventing microcrack nucleation.

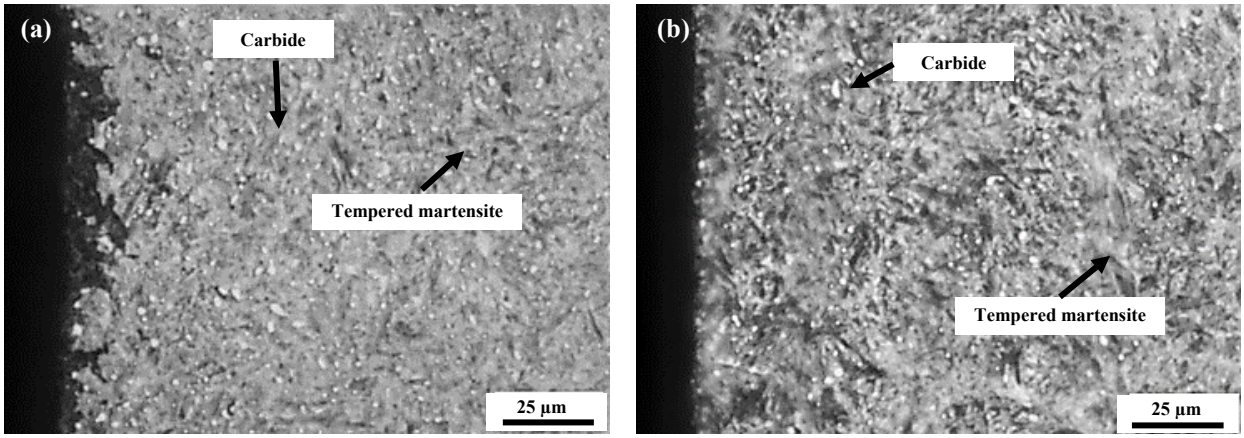


Figure 3. Optical microstructure of SUJ2 after quenching: (a) gas-controlled atmosphere quenching and tempering without polishing (GQT-N), and (b) vacuum quenching and tempering without polishing (VQT-N).

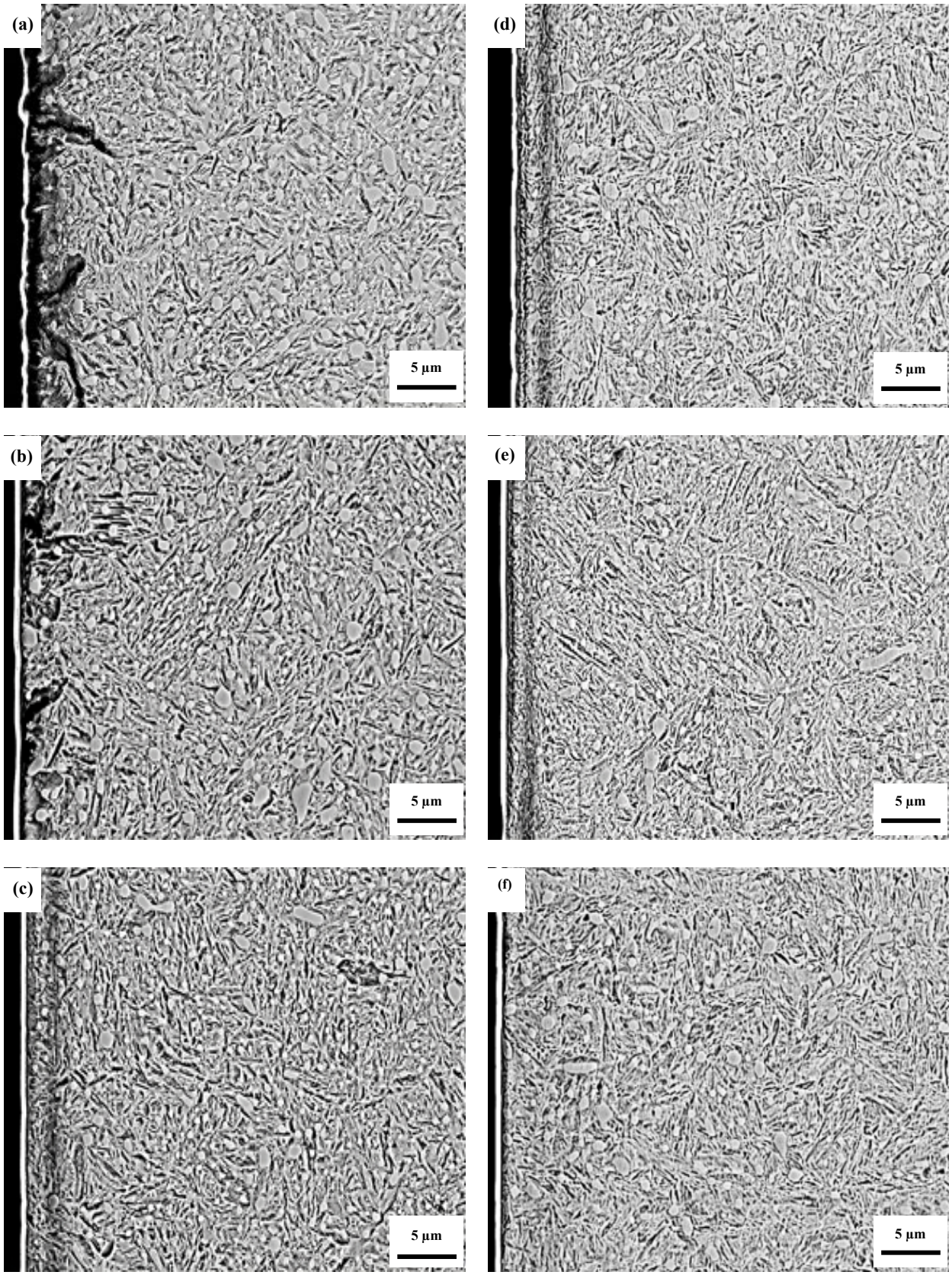


Figure 4. Cross-sectional SEM micrographs of SUJ2 after quenching and coating: (a) GQT-N, (b) GQT-P, (c) GQT-PM, (d) VQT-N, (e) VQT-P, and (f) VQT-PM.

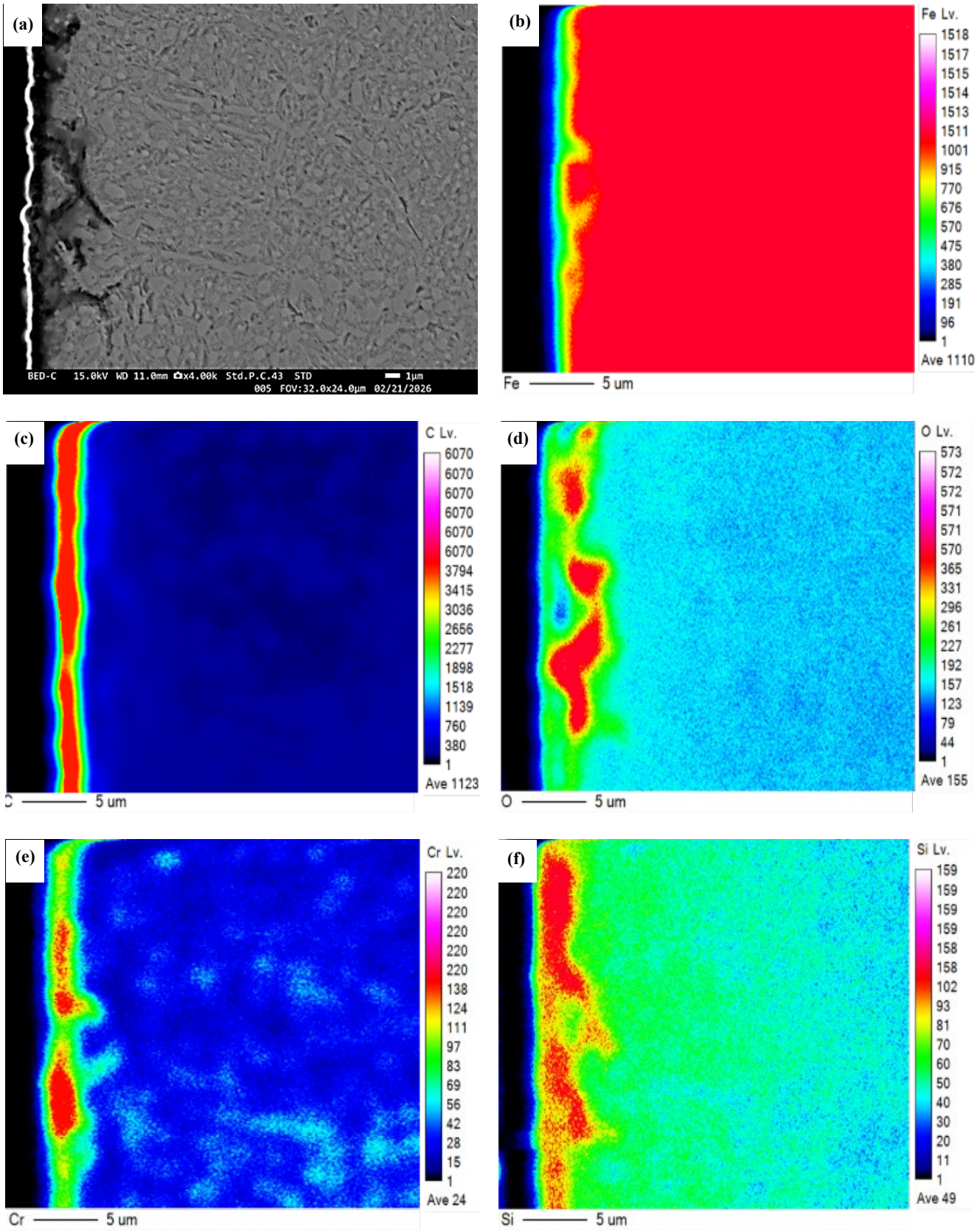


Figure 5. Cross-sectional microstructure at the interface region of JIS SUJ2 steel after quenching and tempering under the GQT-N condition, and spatial elemental distribution analysis using Electron Probe Microanalysis (EPMA): (a) SEM cross-sectional image showing microcracks near the surface, and corresponding elemental mapping of (b) Fe, (c) C, (d) O, (e) Cr, and (f) Si.

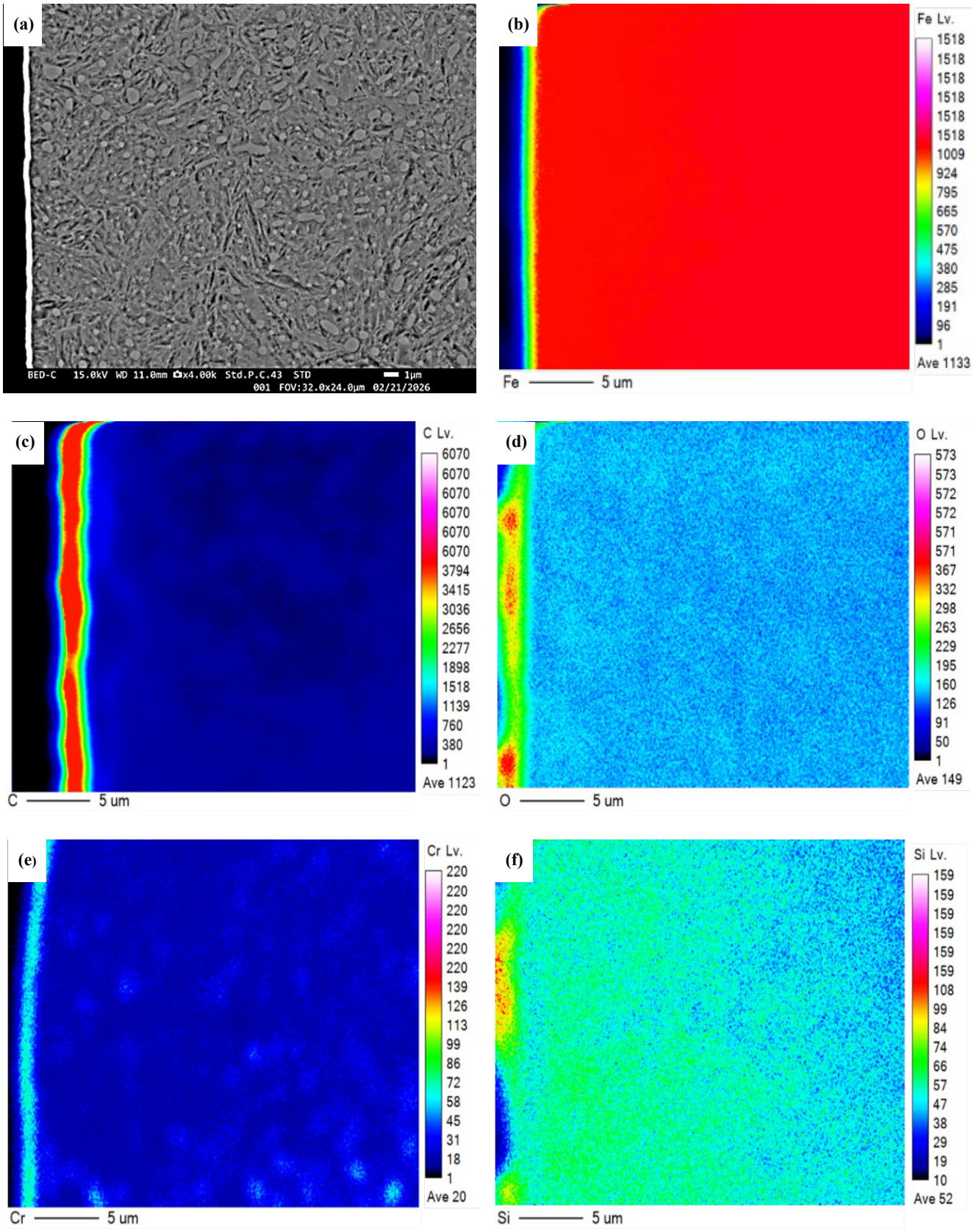


Figure 6 Cross-sectional microstructure at the interface region of JIS SUJ2 steel after quenching and tempering under the VQT-N condition, and spatial elemental distribution analysis using Electron Probe Microanalysis (EPMA): (a) SEM cross-sectional image showing microcracks near the surface, and corresponding elemental mapping of (b) Fe, (c) C, (d) O, (e) Cr, and (f) Si.

3.2 Raman spectroscopy

Raman spectra of the DLC-coated specimens subjected to GQT and VQT hardening processes, combined with different surface preparation conditions (GQT-N, VQT-N, GQT-PM, and VQT-PM), are presented in Figure 7. The spectra exhibit two characteristic peaks corresponding to the disorder-induced D band (~1350 cm^{-1}) and the graphite G band (~1580 cm^{-1}). The emergence of these distinct bands is in excellent agreement with well-established literature [2,13–16], thereby verifying the successful synthesis of amorphous carbon network structures across all experimental groups.

The results indicate that the D band intensity of the GQT specimen without polishing (GQT-N) is the lowest compared to the other samples. This behaviour can be attributed to the influence of surface non-uniformity and the presence of microcracks induced during the gas-quenching process, which affect the nucleation and growth mechanisms of the DLC coating. As substantiated by previous studies [13,14,17], highly irregular surface topologies and structural defects alter the local nucleation energy barrier. This energetic shift modifies the sub-surface atomic hybridization, specifically altering the ratio of sp^2 to sp^3 bonded carbon configurations, which macroscopically manifests as a suppressed D band intensity.

Conversely, the D and G band profiles of the remaining cohorts (VQT-N, GQT-PM, and VQT-PM) display comparable intensities and line shapes. This structural homogeneity indicates that once the surface defects are either eliminated via low-pressure quenching (VQT) or mechanically mitigated through mechanical polishing (PM), the structural integrity and phase composition of the deposited DLC matrix remain remarkably stable.

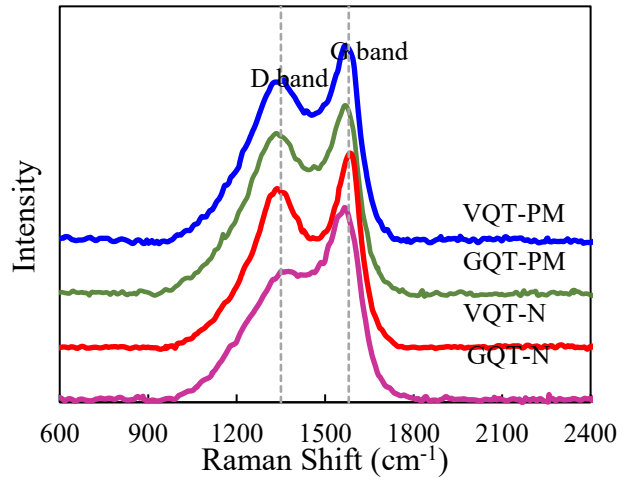


Figure 7. Comparison Raman shift results among GQT-N, VQT-N, GQT-PM, and VQT-PM specimens

3.3 Roughness

The surface roughness analysis of the specimens is presented in Table 2. The results show that the raw material exhibits an average surface roughness of approximately Ra ≈ 0.20 µm. After the hardening process, the surface roughness of the specimens increases, with the GQT process resulting in significantly higher roughness compared to the VQT process. Following surface preparation by polishing, the surface roughness is reduced to approximately Ra ≈ 0.20 µm, which is comparable to that of the raw material. However, after the deposition of the DLC coating, the surface roughness tends to increase again for all specimens. The GQT process results in the highest surface roughness, which can be attributed to the formation of microcracks on the specimen surfaces. In contrast, the VQT process leads to only a slight increase in surface roughness due to minor surface oxidation. In addition, the DLC coating itself contributes to a slight increase in surface roughness. As extensively documented in literature [7,17–21], the plasma-enhanced deposition environment inherently promotes the formation of macro-particles or 'droplets' that protrude from the growing film surface. The accumulation of these microscopic growth defects, which is a well-recognized characteristic of hybrid PVD/PE-CVD processes, contributes to the slight but ubiquitous increase in surface roughness observed after final DLC encapsulation.

3.4 Hardening hardness

The hardness test results of the specimens after gas-quenched treating (GQT) and vacuum-quenched treating (VQT) processes are shown in Figure 8. The results indicate that the hardness values obtained from both processes are comparable, with an average hardness of approximately 745 HV. These findings suggest that there is no significant difference in the hardening capability between the two processes under the given experimental conditions. Both GQT and VQT are able to provide equivalent mechanical properties in terms of material hardness. The observed macro-mechanical behaviour is consistent with the optical microscopy results discussed earlier, which revealed that both thermal treatment routes successfully produced a microstructure predominantly composed of tempered martensite and spheroidized carbides. According to established metallurgical principles and previous studies [6], the overall hardness of low-alloy bearing steels is primarily governed by the carbon dissolved in the martensitic matrix together with the volume fraction of secondary carbides, rather than by the quenching atmosphere pressure itself. Therefore, although the quenching atmosphere significantly influences surface integrity as evidenced by the microcrack formation observed in the GQT specimens both GQT and VQT processes are capable of achieving comparable macroscopic mechanical properties.

Table 2. Comparison of surface roughness values of specimens before and after DLC coating.

Test specimen	Before DLC coating	After DLC coating
RM	0.20 µm ±0.01	0.25 µm ±0.02
GQT-N	0.40 µm ±0.04	0.45 µm ±0.04
GQT-P	0.20 µm ±0.01	0.25 µm ±0.02
GQT-PM	0.20 µm ±0.01	0.25 µm ±0.02
VQT-N	0.30 µm ±0.02	0.35 µm ±0.02
VQT-P	0.20 µm ±0.01	0.25 µm ±0.02
VQT-PM	0.20 µm ±0.01	0.25 µm ±0.02

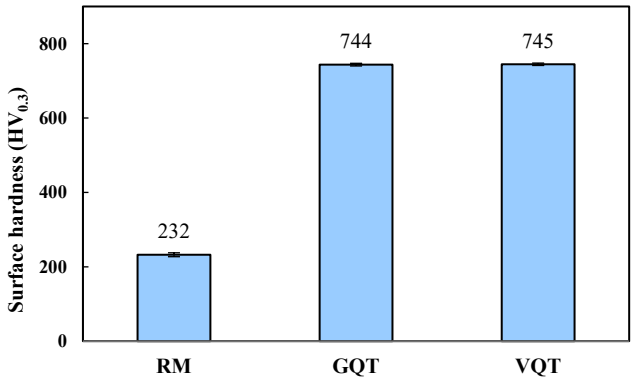


Figure 8. Comparison of hardness after hardening among RM, GQT, and VQT specimens.

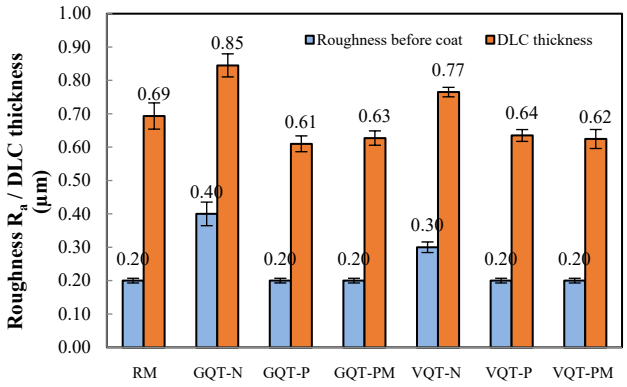


Figure 10. Comparison of DLC coating thickness and roughness before coat on the specimens.

3.5 Hardness of DLC coating

The hardness of the DLC coatings under different hardening and surface preparation conditions is presented in Figure 9. The results show that the raw material and thegas-quenched specimen without polishing (GQT-N) specimen exhibit similar hardness values, in the range of approximately 1300 HV to 1350 HV. In contrast, the other specimens show significantly higher hardness values, ranging from approximately 1650 HV to 1750 HV. These results indicate that the initial substrate hardness prior to DLC coating has a strong influence on the resulting coating hardness. In addition, surface conditions particularly the presence of microcracks also affect the mechanical properties of the DLC coatings. The GQT specimen without polishing (GQT-N), which contains microcracks on the surface, exhibits lower coating hardness compared to the other specimens. This behavior is consistent with the Raman shift analysis, where the GQT specimen without polishing (GQT-N) shows a lower D-band intensity than the other samples. As corroborated by established thin-film growth models [17,21], localized surface non-uniformities and structural defects severely alter the local nucleation energy barrier during the initial stages of deposition. This energetic disruption alters the atomic growth kinetics, shifting the hybridization balance toward a higher sp^2 (graphitic) to sp^3 (diamond-like) bonding ratio. The resulting proliferation of the softer sp^2 phase within the amorphous carbon matrix, induced by the defective substrate topography, ultimately accounts for the macroscopic reduction in coating hardness observed in the GQT-N specimens.

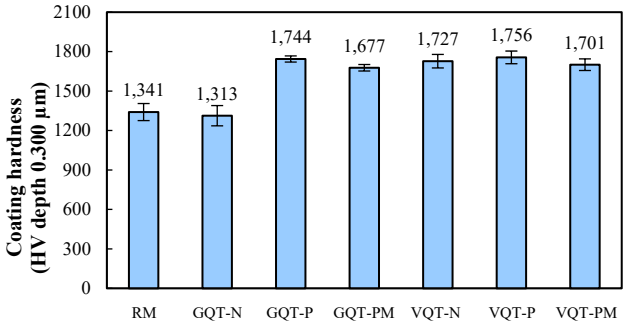


Figure 9. Comparison of DLC coating hardness of specimens measured by a dynamic ultra-microhardness tester depth 0.300 µm.

3.6 DLC coating thickness

The thickness analysis of the DLC coatings is presented in Figure 10. The results indicate that the coating thickness is directly correlated with the surface roughness of the specimens. Specifically, specimens with higher surface roughness exhibit greater coating thickness. The GQT specimen without polishing (GQT-N) and the VQT specimen without polishing (VQT-N) show coating thicknesses of approximately 0.85 µm and 0.77 µm, respectively, which are significantly higher than those of the other specimens. In contrast, specimens with similar surface roughness values exhibit comparable coating thicknesses of approximately 0.65 µm.

According to established thin-film deposition theories [17], the significant influence of surface topography on coating growth is closely associated with the energetic condition of the substrate surface. Surface asperities, peaks, valleys, and micro-defects serve as high-energy preferential nucleation sites, effectively reducing the activation energy required for film formation. As a result, localized deposition rates are enhanced, promoting accelerated film growth at specific microscopic regions. Although these rough surface features contribute to an increase in the overall coating thickness, the growth behavior becomes inherently anisotropic and spatially non-uniform. This localized deposition acceleration therefore leads to considerable thickness variation across the microscale, explaining the thicker yet less homogeneous coating structures observed in both the GQT-N and VQT-N specimens.

3.7 Adhesion properties

The adhesion performance of the deposited DLC coatings was quantitatively assessed using scratch testing, in which the critical load parameters were systematically determined. Following established adhesion evaluation standards [5,22–24], the first critical load Lc1 is defined as the point at which initial cracking occurs, while the second critical load Lc2 corresponds to the point of complete coating delamination. From the SEM microscopic analysis, the Lc1 point was identified by the early appearance of localized tensile horseshoe cracks along the scratch track without exposing the substrate. Conversely, the Lc2 point was characterized by complete coating spallation and delamination along the wear track, clearly revealing the steel substrate beneath.

The results indicate that Lc1 is correlated with the surface roughness of the specimens. Specifically, an increase in surface roughness leads to a higher coating thickness, which enhances the overall stress dissipation capability during contact loading, thereby delaying the onset of Lc1. Furthermore, as the diamond indenter traverses the unpolished substrate, a portion of the lateral shear force is transferred and redistributed along the roughness (peak and valleys) of the substrate, rather than building up into localized, planar tensile stress fields as seen on a smooth interface. Consequently, a higher critical load (Lc1) is required to initiate the first observable microcrack. The GQT and VQT specimens without polishing, which exhibit higher surface roughness, show higher Lc1 values Figure 11 In contrast, specimens with similar surface roughness values exhibit comparable Lc1 values.

For Lc2, the results show a strong correlation with the substrate hardness prior to DLC coating. Specimens with lower initial hardness, such as the raw material, exhibit the lowest Lc2 values Figure 12, indicating inferior adhesion performance. In addition, the hardness of the DLC coating itself also influences Lc2. This is evident in the GQT-N, which has lower coating hardness and consequently exhibits a reduced Lc2 value Figure 13. Considering the effect of the hardening process, the VQT process provides better adhesion performance compared to the GQT process, particularly in cases where surface preparation by polishing is applied to reduce or eliminate microcracks Figure 14. This improvement is attributed to a more uniform surface and the reduction of crack initiation sites, resulting in enhanced overall coating adhesion.

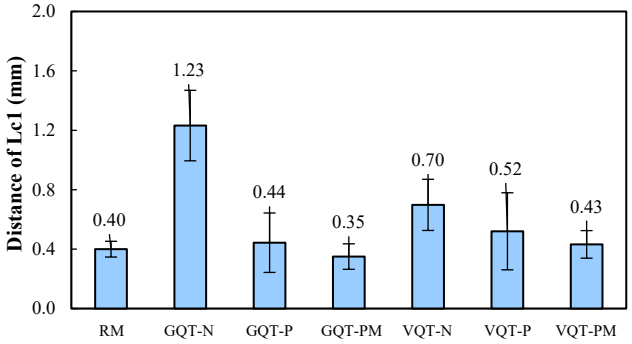


Figure 11. Comparison Lc1 of DLC coating's adhesion on the specimens.

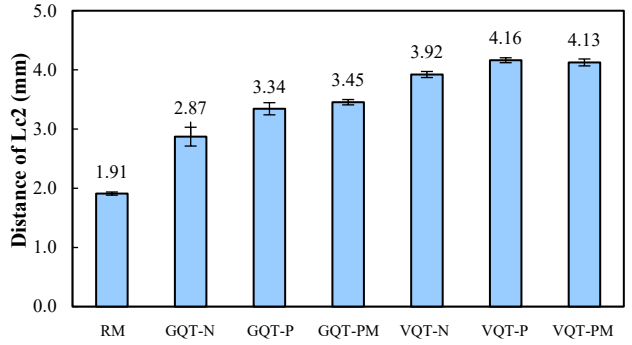


Figure 12. Comparison Lc2 of DLC coating's adhesion on the specimens.

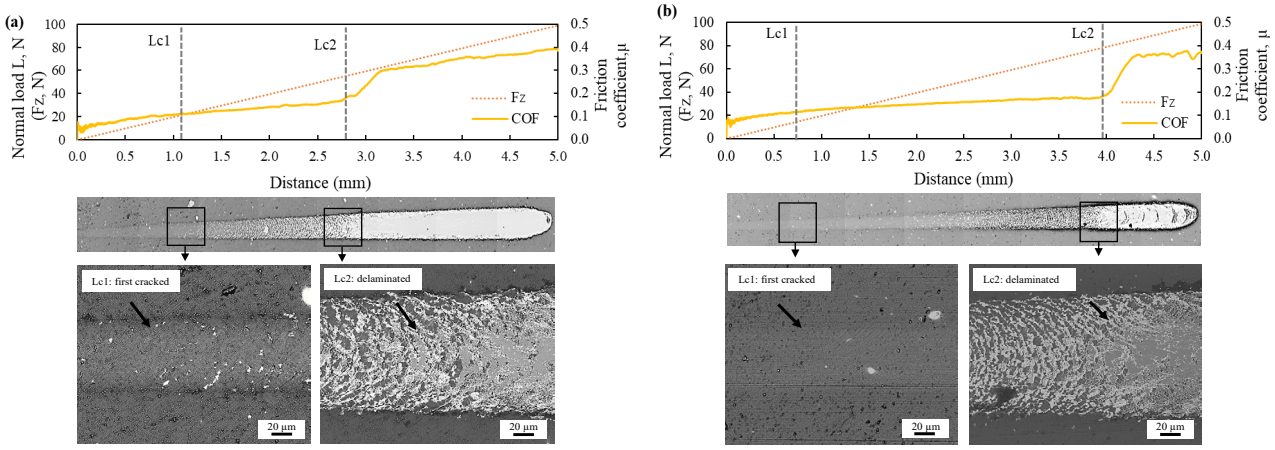


Figure 13. Progressive load scratch test data for DLC coating of: (a) GQT-N, and (b) VQT-N.

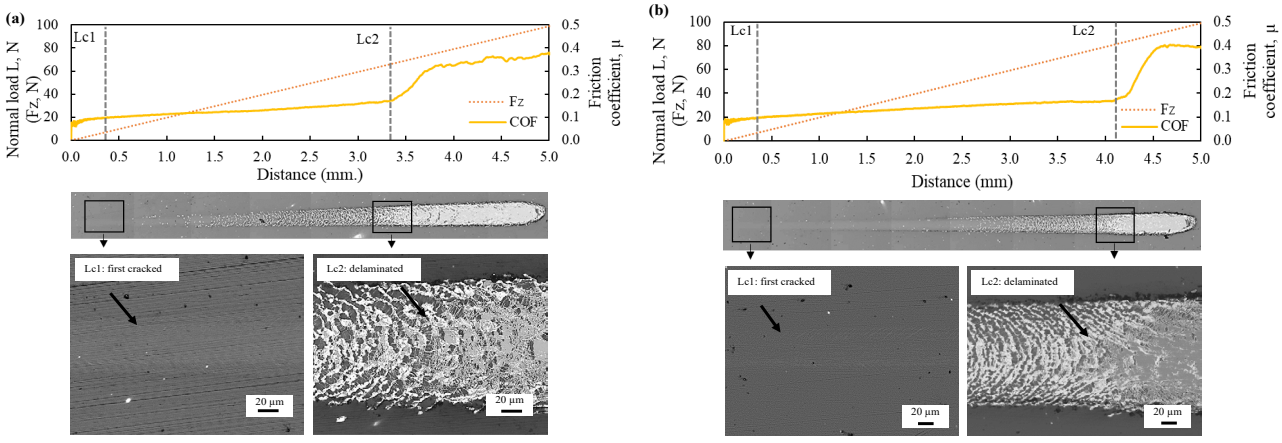


Figure 14. Progressive load scratch test data for DLC coating of: (a) GQT-PM, and (b) VQT-PM.

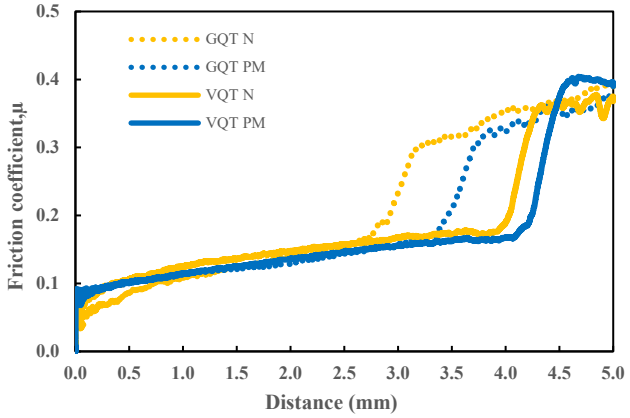


Figure 15. Comparison of coefficient of friction (COF) profiles recorded during progressive loading scratch tests (0–5 mm scratch distance) for DLC coatings on different substrate conditions.

To further evaluate the tribological stability [25] and frictional response under sliding contact, the coefficient of friction (COF) profiles recorded along the 0 to 5 mm scratch length was analysed, as presented in Figure 15. Prior to coating failure, all DLC-coated specimens exhibited a characteristic, steady COF (≈ 0.10 to 0.15), confirming the intrinsic low-friction behaviour of the DLC film. However, the onset of coating delamination (Lc2) induced distinct frictional transitions depending on the surface preparation and hardening method. For all specimens, the COF gradually increased along the scratch track until reaching Lc2, where an abrupt spike occurred. These frictional spikes correspond to severe coating spallation, which exposed the bare steel substrate to direct diamond contact and triggered severe abrasive wear. Although the failure characteristics at Lc2 were similar across all conditions, the polished low-pressure quenched specimen (VQT-PM) maintained the smoothest and most stable COF profile across the entire loading range. The delayed occurrence of COF spikes in VQT-PM directly reflects superior resistance to interfacial spallation, demonstrating that enhanced adhesion effectively translates into improved short-term frictional stability under high contact stress.

4. Conclusions

This study investigates the effects of gas-controlled atmosphere quenching (GQT) and vacuum quenching (VQT), combined with different surface preparation conditions, on microstructure, Raman shift, surface roughness, coating thickness, hardness of DLC coatings, and coating adhesion. Particular emphasis is placed on the influence of microcracks and surface conditions on coating performance. The main conclusions can be summarized as follows:

(1) Both GQT and VQT processes yield similar substrate hardness values (~745 HV), indicating no significant difference in hardening efficiency between the two methods.

(2) Surface microcracks are observed only in specimens treated by GQT, which are attributed to the formation of an internal oxidation layer near the material surface during the quenching process.

(3) Microcracks do not affect the presence of the main Raman peaks (D and G bands are observed in all samples); however, they lead to a reduction in D band intensity. This is due to non-uniform coating growth on rough and cracked surfaces, resulting in increased surface roughness and reduced DLC coating hardness, associated with a more disordered film structure.

(4) Surface roughness and the presence of microcracks directly influence the thickness of the DLC coatings. Rough surfaces promote nucleation and localized film growth, particularly at surface asperities, leading to increased coating thickness but with greater non-uniformity compared to smoother surfaces.

(5) Coating adhesion is related to the mechanical properties of both the coating and the substrate. Coatings with lower hardness tend to exhibit higher Lc1 values due to greater toughness and better resistance to crack initiation. In contrast, higher coating and substrate hardness contribute to higher Lc2 values, indicating improved resistance to delamination and scratch failure.

In summary, although GQT and VQT produce comparable substrate hardness, differences in surface conditions, particularly microcrack formation and surface roughness play a critical role in determining the structure, properties, and overall performance of DLC coatings. Therefore, careful control of surface conditions prior to coating is essential to achieve optimal coating performance.

Acknowledgements

The authors gratefully acknowledge Thai Tohken Thermo Co., Ltd. and Chulalongkorn University for their provision of materials, equipment, facilities, and technical support. The authors also express their sincere appreciation to Dr. Sankum Nusen and Dr. John T.H. Pearce of Chiang Mai University, Thailand, for their valuable insights and constructive discussions.

References

[1] C. P. O. Treutler, "Industrial use of plasma-deposited coatings for components of automotive fuel injection systems," *Surface and Coatings Technology*, vol. 200, no. 5–6, pp. 1969–1975, 2005.

[2] E. Humali, G. Hizli, and K. Kazmanli, "Optical behavior of multilayer DLC films produced by periodically altered RF voltage: Experimental and theoretical model," *Optical Materials*, vol. 169, Art. no. 117556, 2026.

[3] A. Rockett, The Materials Science of Semiconductors. 2008.

[4] J. A. Thornton, "Influence of apparatus geometry and deposition conditions on the structure and topography of thick sputtered coatings," *Journal of Vacuum Science and Technology*, vol. 11, no. 4, pp. 666–670, 1974.

[5] Y. Xu, Y. Wu, J. Wang, T. Zhang, Y. Chen, and Y. Liu, "Effect of the Cr/Cr-C sublayer on the adhesional strength and tribological properties of DLC film," *Surface and Coatings Technology*, vol. 519, Art. no. 132948, 2026.

[6] C. A. Stickels, "Carbide refining heat treatments for 52100 bearing steel," *Metallurgical transactions*, vol. 5, pp. 865–874, 1973.

[7] P. Harlin, P. Carlsson, U. Bexell, and M. Olsson, "Influence of surface roughness of PVD coatings on tribological performance in sliding contacts," *Surface and Coatings Technology*, vol. 201, no. 7, pp. 4253–4259, 2006.

[8] N. Konkhunthot, C. Euaruksakul, P. Photongkam, and P. Wongpanya, "Characterization of diamond-like carbon (DLC)

films deposited by filtered cathodic vacuum arc technique," *Journal of Metals, Materials and Minerals*, vol. 23, no. 1, pp. 35–40, 2013.

[9] R. Chatterjee-Fischer, "Internal oxidation during carburizing and heat treating," *Metallurgical Transactions A*, vol. 9, pp. 1553–1560, 1978.

[10] I. S. Kozlovskii, A. T. Kalinin, a. A. I. F. A. Ya. Novikova, and E. A. Lebedeva, "Metal sceience and heat treatment," *Metallovdenie i Termicheskaya Obrabotka Metallov*, no. 3, pp. 2–7, 1967.

[11] A. Stormvinter, H. Kristoffersen, E. Troell, J. Senaneuch, and S. Haglund, "Impact of internal oxidation and quenching path on fatigue of powertrain components," presented at the heat treat 2015: Proceedings from the 28th Heat Treating Society Conference, 2015.

[12] C. Mao, T. Zeng, Y. Hu, D. Zhang, M. Zhang, W. Wang, J. Gong, W. Tang, Y. Luo, Z. M. Bi, "A comparative study on microstructure evolution of metamorphic layers induced by grinding and laser quenching in hardened AISI 52100 steel," *Surface and Coatings Technology*, vol. 507, Art. no. 132142, 2025.

[13] E. C. T. Ba, M. R. Dumont, P. S. Martins, B. da Silva Pinheiro, M. P. M. da Cruz, and J. W. Barbosa, "Deconvolution process approach in Raman spectra of DLC coating to determine the sp3 hybridization content using the ID/IG ratio in relation to the quantification determined by X-ray photoelectron spectroscopy," *Diamond and Related Materials*, vol. 122, Art. no. 108818, 2022.

[14] R. Yuan, Y. Guo, I. Gurgan, N. Siddique, Y. Li, S. Jang, G. Noh, H. Kim, "Raman spectroscopy analysis of disordered and amorphous carbon materials: A review of empirical correlations," *Carbon*, vol. 238, Art. no. 120214, 2025.

[15] W. G. Cui, Q. B. Lai, L. Zhang, and F. M. Wang, "Quantitative measurements of sp^3 content in DLC films with Raman spectroscopy," *Surface and Coatings Technology*, vol. 205, no. 7, pp. 1995–1999, 2010.

[16] A. Habibi, S. M. Mousavi Khoie, F. Mahboubi, and M. Urgen, "Raman spectroscopy of thin DLC film deposited by plasma electrolysis process," *Surface and Coatings Technology*, vol. 309, pp. 945–950, 2017.

[17] F. C. Dalan, A. S. da Silva Sobrinho, L. M. G. da Silva, S. F. Santos, A. R. Marcondes, and K. R. Cardoso, "Effect of substrate roughness on AlCoCrFeNiNb0.6 HEA coating growth, adhesion and wear behavior," *Surface and Coatings Technology*, vol. 523, Art. no. 133248, 2026.

[18] M. HagarovÃ¡, D. JakubÃ©czyovÃ¡, and M. Vojtko, "PVD coatings applied on the tool steels," *Journal of Metals, Materials and Minerals*, vol. 17, no. 1, pp. 29–33, 2007.

[19] M. Hagarová, "Structure and Properties of thin layer – Substrate on high speed steel with different thickness of TiN," *Journal of Metals, Materials and Minerals,* vol. 15, no. 2, pp. 39–43, 2005.

[20] C. Chokwatvikul, S. Larpkiattaworn, S. Surinphong, C. Busabok, and P. Termsuksawad, "Effect of nitrogen partial pressure on characteristic and mechanical properties of hard coating TiAlN film," *Journal of Metals, Materials and Minerals*, vol. 21, no. 1, pp. 115–119, 2011.

[21] M.-R. Ardigo-Besnard, A. Besnard, G. Nkou Bouala, P. Boulet, Y. Pinot, and Q. Ostorero, "Effect of pre-oxidation on a Ti PVD coated ferritic steel substrate during high-temperature aging," *Crystals*, vol. 12, no. 12, Art. no. 1732, 2022.

[22] B. Waseem, S. Alam, M. Irfan, M. Shahid, M. Farooq, B. D. Soomro, S. Hashim, R. Iqbal, "Optimization and characterization of adhesion properties of DLC coatings on different substrates," *Materials Today: Proceedings,* vol. 2, no. 10, pp. 5308–5312, 2015.

[23] H. Ju, L. Yu, D. Yu, I. Asempah, and J. Xu, "Microstructure, mechanical and tribological properties of TiN-Ag films deposited by reactive magnetron sputtering," *Vacuum*, vol. 141, pp. 82–88, 2017.

[24] S. A. Siddiqui, G. Favaro, and M. Berkes Maros, "Investigation of the damage mechanism of CrN and diamond-like carbon coatings on precipitation-hardened and duplex-treated $X_{42}Cr_{13}$/W tool steel by 3D scratch testing," *Journal of Materials Engineering and Performance*, vol. 31, no. 10, pp. 7830–7842, 2022.

[25] H. S. Maurya, J. Jayaraj, Z. Wang, K. Juhani, F. Sergejev, and K. G. Prashanth, "Investigation of the tribological behavior of the additively manufactured TiC-based cermets by scratch testing," *Journal of Alloys and Compounds*, vol. 959, Art. no. 170496, 2023.